BIOCHEMISTRY
including biophysical chemistry & molecular biology

Article

pubs.acs.org/biochemistry

Variable Active Site Loop Conformations Accommodate the Binding of Macrocyclic Largazole Analogues to HDAC8

Christophe Decroos,[†] Dane J. Clausen,[‡] Brandon E. Haines,[§] Olaf Wiest,[§,∥] Robert M. Williams,[‡,⊥] and David W. Christianson*[,†]

[†]Roy and Diana Vagelos Laboratories, Department of Chemistry, University of Pennsylvania, Philadelphia, Pennsylvania 19104-6323, United States

[‡]Department of Chemistry, Colorado State University, Fort Collins, Colorado 80523, United States

[§]Department of Chemistry and Biochemistry, University of Notre Dame, Notre Dame, Indiana 46556, United States

[∥]Laboratory of Computational Chemistry and Drug Design, Laboratory of Chemical Genomics, Peking University Shenzhen Graduate School, Shenzhen 518055, China

[⊥]University of Colorado Cancer Center, Aurora, Colorado 80045, United States

ABSTRACT: The macrocyclic depsipeptide Largazole is a potent inhibitor of metal-dependent histone deacetylases (HDACs), some of which are drug targets for cancer chemotherapy. Indeed, Largazole partially resembles Romidepsin (FK228), a macrocyclic depsipeptide already approved for clinical use. Each inhibitor contains a pendant side chain thiol that coordinates to the active site Zn^{2+} ion, as observed in the X-ray crystal structure of the HDAC8−Largazole complex [Cole, K. E., Dowling, D. P., Boone, M. A., Phillips, A. J., and Christianson, D. W. (2011) *J. Am. Chem. Soc. 133*, 12474]. Here, we report the X-ray crystal structures of HDAC8 complexed with three synthetic analogues of Largazole in which the depsipeptide ester is replaced with a rigid amide linkage. In two of these analogues, a six-membered pyridine ring is also substituted (with two different orientations) for the five-membered thiazole ring in the macrocycle skeleton. The side chain thiol group of each analogue coordinates to the active site Zn^{2+} ion with nearly ideal geometry, thereby preserving the hallmark structural feature of inhibition by Largazole. Surprisingly, in comparison with the binding of Largazole, these analogues trigger alternative conformational changes in loops L1 and L2 flanking the active site. However, despite these structural differences, inhibitory potency is generally comparable to, or just moderately less than, the inhibitory potency of Largazole. Thus, this study reveals important new structure−affinity relationships for the binding of macrocyclic inhibitors to HDAC8.

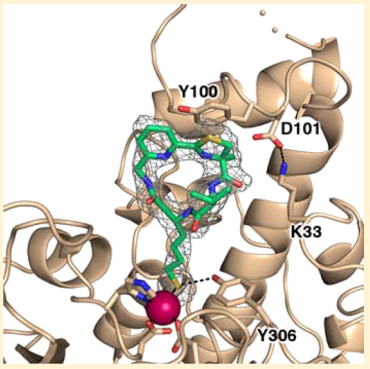

Class I, II, and IV histone deacetylases (HDACs)[1,2] are metal-dependent enzymes that utilize a single transition metal ion, either Zn^{2+} and/or Fe^{2+} *in vivo*,[3] to catalyze the hydrolysis of *trans*-acetyl-L-lysine residues[4] in histone and non-histone proteins to regulate their function.[5,6] These enzymes, also known more broadly as lysine deacetylases, are critical targets for inhibitor design because they are implicated in a variety of biological processes such as gene expression, cellular differentiation, proliferation, and apoptosis.[7−11] Upregulated HDAC activity is associated with tumorigenesis, and the HDAC inhibitors suberoylanilide hydroxamic acid (Zolinza)[12,13] and Romidepsin (Istodax)[14,15] are currently in clinical use for cancer chemotherapy.

Romidepsin (Figure 1) is particularly notable among HDAC inhibitors in that it is a macrocyclic depsipeptide that undergoes disulfide reduction *in vivo* to liberate an ∼7 Å thiol side chain that coordinates to the active site metal ion. Although no X-ray crystal structure of an HDAC−Romidepsin complex has been reported to date, the crystal structure of HDAC8 complexed with the active form of a structurally related marine natural product, Largazole thiol [henceforth simply termed "Largazole" (Figure 1)],[16,17] reveals that the thiol side chain is readily accommodated in the narrow tunnel that otherwise accommodates the substrate *trans*-acetyl-L-lysine.[18] The thiol moiety of Largazole is presumably ionized as the negatively charged thiolate to coordinate to the active site Zn^{2+} ion, and ideal metal coordination geometry contributes to exceptionally high affinity.[18] Indeed, Largazole is one of the most potent HDAC inhibitors known and exhibits low nanomolar affinity against several HDAC isozymes.[17,19] A key difference between Largazole and Romidepsin is that the 16-membered depsipeptide ring of Largazole contains an unusual thiazoline−thiazole moiety, suggesting potential opportunities for the design of diverse macrocyclic analogues.

Among the total syntheses of Largazole reported soon after its discovery,[17,20−22] Williams and colleagues reported a modular and scalable total synthesis that facilitated the generation of Largazole analogues containing modified thiol

Received: January 5, 2015
Revised: March 6, 2015
Published: March 20, 2015

ACS Publications © 2015 American Chemical Society

DOI: 10.1021/acs.biochem.5b00010
Biochemistry 2015, 54, 2126−2135

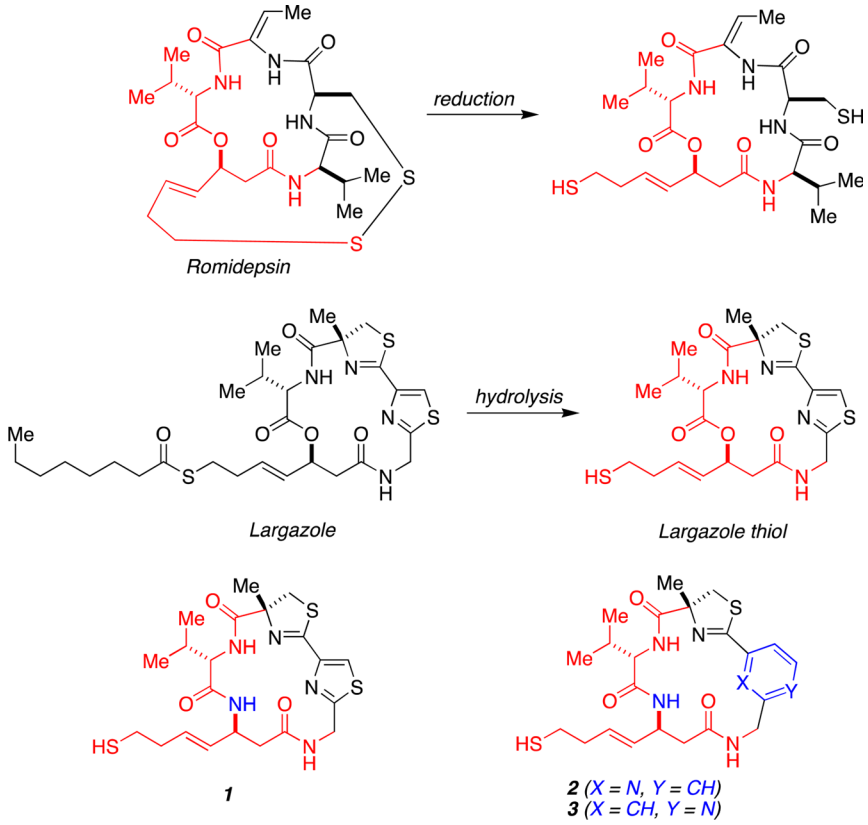

Figure 1. Macrocyclic depsipeptide Romidepsin is an approved drug used for cancer chemotherapy; reduction of the disulfide linkage liberates the active form of the inhibitor. In contrast, the macrocyclic depsipeptide Largazole is activated by hydrolysis of the thioester group to yield the thiol moiety that targets Zn^{2+} coordination (Largazole thiol is termed "Largazole" throughout). Both Romidepsin and Largazole share a core structure (red) that is responsible for potent inhibition of HDAC8. In this study, the Largazole macrocycle has been rigidified by substitution of an amide linkage for the ester linkage in **1**. Further elaboration of this macrocyclic peptide platform by two alternative substitution patterns of a pyridine ring in place of the thiazole ring yields **2** and **3**. Substituted atoms relative to Largazole are colored blue.

side chains,[19] thiazole-pyridine and -oxazole substitutions,[19,23] and a macrocyclic ring in which the depsipeptide ester linkage is rigidified by the substitution of an amide linkage.[24] The thiazole-pyridine substitution is particularly intriguing because this modification confers a 3−4-fold enhancement of inhibitory potency (IC_{50}) against several HDAC isozymes.[19] Conversely, the conversion of the macrocyclic depsipeptide into a macrocyclic peptide generally results in a 3−4-fold loss of inhibitory potency.[24]

To improve our understanding of structure−affinity relationships for Largazole analogues, we now report the high-resolution X-ray crystal structures of three macrocyclic peptide analogues, **1**−**3** (Figure 1), complexed with HDAC8. These structures reveal how the enzyme active site accommodates derivatization of the macrocyclic skeleton and may suggest potential new avenues for modifications that could further modulate biological activity. Among the greater family of HDAC isozymes, HDAC8 is the most amenable to the X-ray crystal structure determination of enzyme−inhibitor complexes, and the crystal structure of the HDAC8−Largazole complex[18] provides an important reference point for the structures described herein. Accordingly, HDAC8 serves as a paradigm for inhibitor design experiments targeting the class I isozymes (HDAC1−3 and -8) that serve as targets for cancer chemotherapy,[7−11] and HDAC8 itself has been recently identified as a target for neuroblastoma chemotherapy.[25]

MATERIALS AND METHODS

Reagents. Most chemicals used for buffers or crystallization were purchased from Fisher or Sigma and used without further purification. The synthesis of compound **1** has been previously described,[24] and the preparations of **2** and **3** are being reported elsewhere.[26]

Crystallization and Determination of the Structure of HDAC8−Inhibitor Complexes. To facilitate crystallization, the S39D mutation was introduced into the previously described HDAC8-6His-pET20b construct[27] according to QuickChange site-directed mutagenesis protocols using forward 5′-CTA AAA TCC CGA AAC GTG CAG ACA TGG TGC ATT CTT TGA TTG AAG-3′ and reverse 5′-CTT CAA TCA AAG AAT GCA CCA TGT CTG CAC GTT TCG GGA TTT TAG-3′ primers. DNA sequencing at the University of Pennsylvania Perelman School of Medicine confirmed the incorporation of the desired mutation. Recombinant S39D HDAC8 was expressed and purified as previously described.[28] As noted by Vannini and colleagues,[29] this mutant is properly folded and catalytically active, but it can also yield higher-quality crystals of enzyme−inhibitor complexes in comparison with those of the wild-type enzyme. Because the structures of wild-type HDAC8 and S39D HDAC8 are essentially identical, we henceforth refer to S39D HDAC8 simply as "HDAC8".

Crystals of HDAC8−inhibitor complexes were prepared by cocrystallization at 4 °C (except for the complex with **3**, which was cocrystallized at 21 °C) in sitting drops using the vapor

DOI: 10.1021/acs.biochem.5b00010
Biochemistry 2015, 54, 2126−2135

diffusion method. In general, a 500 nL drop containing 5 mg/mL HDAC8, 50 mM Tris (pH 8.0), 150 mM KCl, 5% (v/v) glycerol, 1 mM DTT, 0.5 mM tris(2-carboxyethyl)phosphine (TCEP) (except for **1**, which did not require TCEP for cocrystallization), 2 mM inhibitor, 5% (v/v) DMSO, and 0.03 M glycylglycylglycine was added to a 500 nL drop of precipitant solution and equilibrated against a 100 μL reservoir of precipitant solution. The precipitation solution for the cocrystallization of the HDAC8−**1** complex consisted of 100 mM imidazole (pH 7.0), 8% PEG 8000 (Hampton Research), and 4 mM TCEP. The precipitation solution for the cocrystallization of the HDAC8−**2** complex consisted of 100 mM imidazole (pH 7.0), 13% PEG 3350 (Hampton Research), and 4 mM TCEP. Finally, the precipitation solution for the cocrystallization of the HDAC8−**3** complex consisted of 100 mM BisTris (pH 6.5), 8% PEG 3350, and 4 mM TCEP.

Crystals of each complex appeared within 1−2 days and were flash-cooled in liquid nitrogen after transfer to a cryoprotectant solution consisting of precipitant solution supplemented with 25% glycerol for the HDAC8−**1** complex, 30% glycerol for the HDAC8−**2** complex, and 30% of a 1:1 (v/v) mixture of PEG 400 (Hampton Research) and 2-methyl-2,4-pentanediol for the HDAC8−**3** complex. X-ray diffraction data were collected on beamline X29 at the National Synchrotron Light Source (NSLS, Brookhaven National Laboratory, Upton, NY). Data collection statistics are listed in Table 1. Data were indexed, integrated, and scaled using HKL2000.[30]

Analysis of X-ray intensity data collected from crystals of the HDAC8−**3** complex revealed deviations from ideal intensity statistics suggestive of twinning, which is somewhat unusual for crystallographic space group $P2_1$. Intensity statistics can deviate from ideality because of other crystallographic complications, as observed in the structure of the amino acid ester hydrolase from *Acetobacter turbidans*, in which merohedral twinning in space group $P2_1$ was complicated by pseudotranslational noncrystallographic symmetry.[31] For the HDAC8−**3** complex, we reindexed intensity data in space group $P1$ and used Zanuda (contained in the CCP4 suite of programs[32]) to validate the $P2_1$ space group and origin assignments. We proceeded to determine the structure by molecular replacement using PHENIX[33] with the atomic coordinates of the H143A HDAC8−tetrapeptide substrate complex (Protein Data Bank entry 3EWF)[27] less ligand, ion, and solvent used as a search probe for rotation and translation function calculations. Refinement and manual model adjustment were performed with PHENIX and COOT, respectively.[33,34] While the origin of the deviation from ideal intensity statistics remains unknown for these crystals, it is clear that the minor crystallographic defect that might be present in these crystals did not hinder satisfactory refinement based on the refinement statistics listed in Table 1.

X-ray data collected from crystals of the HDAC8 complexes with **1** and **2** exhibited ideal intensity distributions and did not require further analysis. Structures were determined by molecular replacement using PHENIX[33] and refined and rebuilt with PHENIX and COOT, respectively.[33,34] Refinement converged smoothly, and detailed refinement statistics are listed in Table 1.

Certain segments in each structure (the N-terminus, the C-terminus, and a portion of the L2 loop) appeared to be disordered and were accordingly excluded from each final model as follows: HDAC8−**1** complex, M1−S13 (monomers A and B), D87−D92 (monomer A), E85−D89 (monomer B), G99 and Y100 (monomer B), E379−H389 (monomer A), and S383−H389 (monomer B); HDAC8−**2** complex, M1−S13 (monomer A), M1−Q12 (monomer B), D88−P91 (monomer A), E85−D88 (monomer B), Y100 and D101 (monomer B), E379−H389 (monomer A), and I378−H389 (monomer B); and HDAC8−**3** complex, M1−L14 (monomers A and B), E85−D92 (monomer A), G99−A104 (monomer A), D87−D92 (monomer B), and I378−H389 (monomers A and B). Ambiguous electron density was observed for L2 loop segment

Table 1. Data Collection and Refinement Statistics

	HDAC8−**1** complex	HDAC8−**2** complex	HDAC8−**3** complex
	Unit Cell		
space group symmetry	$P2_1$	$P2_1$	$P2_1$
a, b, c (Å)	53.9, 85.0, 94.7	54.1, 85.1, 95.4	53.8, 84.7, 94.1
α, β, γ (deg)	90, 100.3, 90	90, 100.2, 90	90, 100.5, 90
	Data Collection		
wavelength (Å)	1.075	1.075	1.075
resolution limits (Å)	50.0−1.76	50.0−2.18	50.0−2.39
total/unique no. of reflections	621648/82963	273766/44473	195462/32705
R_{merge} [a,b]	0.073 (0.317)	0.124 (0.811)	0.144 (0.736)
$I/\sigma(I)$ [a]	21.3 (7.6)	13.0 (2.8)	12.9 (2.2)
redundancy [a]	7.5 (7.3)	6.2 (6.1)	6.0 (4.5)
completeness (%) [a]	99.9 (100)	100 (100)	98.7 (97.5)
	Refinement		
no. of reflections used in refinement/test set	82933/4145	44415/2238	32682/2526
R_{cryst} [c]	0.137	0.182	0.187
R_{free} [d]	0.162	0.213	0.224
no. of protein atoms [e]	5715	5608	5481
no. of water molecules [e]	750	349	182
no. of ligand molecules [e]	2	2	2
no. of Zn^{2+} ions [e]	2	2	2
no. of K^+ ions [e]	4	4	4
no. of glycerol molecules [e]	1	1	–
no. of imidazole molecules [e]	1	1	–
root-mean-square deviation from ideal geometry			
bonds (Å)	0.010	0.002	0.002
angles (deg)	1.3	0.7	0.6
dihedral angles (deg)	15	11	11
Ramachandran plot (%) [f]			
allowed	91.2	91.2	90.7
additionally allowed	8.8	8.8	9.3
Protein Data Bank entry	4RN0	4RN1	4RN2

[a]Values in parentheses refer to the highest-resolution shell of data. [b]$R_{merge} = \sum|I_h - \langle I\rangle_h|/\sum I_h$, where $\langle I\rangle_h$ is the average intensity calculated from replicate reflections. [c]$R_{cryst} = \sum||F_o| - |F_c||/\sum|F_o|$ for reflections contained in the working set. $|F_o|$ and $|F_c|$ are the observed and calculated structure factor amplitudes, respectively. [d]$R_{free} = \sum||F_o| - |F_c||/\sum|F_o|$ for reflections contained in the test set held aside during refinement. [e]Per asymmetric unit. [f]Calculated with PROCHECK version 3.4.4.

DOI: 10.1021/acs.biochem.5b00010
Biochemistry 2015, 54, 2126−2135

E85−D89 and the G99-Y100 pair and the Y100-D101 pair in monomer B of the HDAC8−**1** and HDAC8−**2** complexes, respectively. Such ambiguous electron density might arise from molecular disorder or multiple conformations, but it was not sufficiently clear to allow a clear interpretation. Accordingly, these short segments were not modeled. Likewise, side chains of residues that were completely disordered were excluded from the model as follows: HDAC8−**1** complex, K60, S93, Q253, and K374 of monomer A and L14, K60, K81, V82, Q84, H90, D92, S93, I94, E95, D101, C102, K132, Q253, and E379 of monomer B; HDAC8−**2** complex, D87, D92, S93, Q253, and E358 of monomer A and S13, E23, K58, K60, K81, Q84, D89, D92, C102, K221, K249, and K374 of monomer B; and HDAC8−**3** complex, K33, K60, D73, K81, I94, E95, T105, E106, and Q253 of monomer A and K33, S93, I94, E95, K325, and E358 of monomer B.

RESULTS

Initial inhibitor cocrystallization experiments with wild-type HDAC8 were unsuccessful. Therefore, the site-specific mutant S39D HDAC8 was utilized for cocrystallization experiments with Largazole analogues **1**−**3**. As noted by Vannini and colleagues,[29] this mutant is properly folded and catalytically active, but it can also yield higher-quality crystals of enzyme−inhibitor complexes in comparison with those of the wild-type enzyme because of additional crystal contacts. The side chain of S39 is ∼20 Å from the active site and undergoes phosphorylation by cyclic AMP-dependent protein kinase A.[35] However, the structures of wild-type HDAC8 and S39D HDAC8 are essentially identical, so inhibitor binding modes are expected to be similarly identical in each enzyme active site. Accordingly, we henceforth refer to S39D HDAC8 simply as "HDAC8".

In the structure of each enzyme−inhibitor complex, the Largazole analogue binds to monomers A and B in the asymmetric unit with full occupancy and thermal *B* factors comparable to those of surrounding residues. The thiol side chain of each inhibitor extends into the narrow active site tunnel and coordinates to the Zn^{2+} ion, presumably as the negatively charged thiolate. This is the hallmark of HDAC inhibition by Largazole, and these structures reveal that ideal thiolate−zinc coordination geometry is conserved in the binding of Largazole analogues. As previously measured by Williams and colleagues,[26] IC_{50} values for Largazole and analogues **1**−**3** are summarized in Table 2. The specific details of each enzyme−inhibitor complex are outlined below.

HDAC8−1 Complex. Largazole analogue **1** is essentially isosteric with Largazole except for the substitution of the cyclic depsipeptide ester with an amide group. The overall structure of the HDAC8−**1** complex determined at 1.76 Å resolution is similar to that of the wild-type HDAC8−Largazole complex [root-mean-square deviations (rmsds) of 0.58 Å for 350 Cα atoms and 0.29 Å for 345 Cα atoms in monomers A and B, respectively]. An electron density map of the enzyme−inhibitor complex (Figure 2a) reveals that the geometry of thiolate−Zn^{2+} coordination is nearly ideal[36] with an average S−Zn^{2+} distance of 2.3 Å, a C−S−Zn^{2+} angle of 101°, and a C−C−S−Zn^{2+} dihedral angle of 95° (values averaged over monomers A and B). Additionally, the phenolic side chain of Y306 donates a hydrogen bond to the Zn^{2+}-bound thiolate anion. The Zn^{2+} ion is coordinated with distorted tetrahedral geometry (average ligand−Zn^{2+}−ligand angles in the range of 98−119°).

Notably, the ester-to-amide substitution in the macrocyclic peptide moiety of **1** results in a slight conformational difference, in that the average dihedral angle of the ester linkage of Largazole is 171° for the ester and 180° for the amide. The higher energetic barrier for the distortion of an amide compared with an ester serves to rigidify this linkage with a planar conformation. However, comparison of the HDAC8−**1** complex with the wild-type HDAC8−Largazole complex reveals that this conformational difference is readily tolerated and does not perturb the overall binding mode of the macrocycle. Even so, while the macrocycle conformations of Largazole and **1** are essentially identical (rmsd of 0.32 Å for the 32 non-hydrogen atoms of each inhibitor), the macrocycle pivots by ∼25° around an axis roughly defined by the Zn^{2+}-bound thiolate and the thiazole−thiazoline bond as the structures of the two enzyme−inhibitor complexes are superimposed (Figure 2b).

Surprisingly, major structural differences are observed in the L1 and L2 loops that accommodate the slightly pivoted binding orientation of **1**. Whereas D101 in the L2 loop hydrogen bonds with Largazole, the L2 loop in the HDAC8−**1** complex adopts an alternative conformation such that D101 is more than 7 Å from **1**. Instead, adjacent residue Y100 (L2 loop) tends toward a van der Waals interaction with **1**, and D101 accepts hydrogen bonds from K33 (L1 loop) and Y154 (Figure 2b). Additionally, K33 of monomer B hydrogen bonds with the carbonyl group close to the thiazoline group of **1** in both monomers A and B. This interaction can be relevant in monomer B only in solution because HDAC8 is a monomer.

Interestingly, the structures of monomers A and B are not exactly identical (rmsd of 0.59 Å for 351 Cα atoms); in particular, significant structural differences are observed for loops L1 and L2 (Figure 3a). Although **1** binds similarly in each monomer, portions of the L2 loop of each monomer adopt different conformations, and the L2 loop in monomer B is more disordered than in monomer A: the E85−H90 and D99−Y100 segments are not modeled because of ambiguous or missing electron density presumably caused by disorder. However, certain modeled segments of the L2 loop clearly exhibit alternative conformations. The most significant structural difference is observed for T105, which moves by 9 Å between monomers A and B because of the partial unwinding of helix B4. These structural differences propagate to the L1 loop, where L31 moves by more than 3 Å, and helix B2, where the V82−Q84 segment shifts by ∼2.5 Å.

Finally, we note that the peptide macrocycle of **1** makes several solvent-mediated hydrogen bond interactions with active site residues that may contribute to inhibitory activity (Figure 3b). These hydrogen bond networks generally involve one to three intervening water molecules. Interestingly, an imidazole molecule from the crystallization buffer interacts with a peptide carbonyl group of **1** [monomer A only (not shown)]. Some, but not all, enzyme−solvent−inhibitor hydrogen bond

Table 2. Inhibitory Activity of Largazole Analogues against Class I HDACs (IC_{50}, nM)[a]

	HDAC1	HDAC2	HDAC3	HDAC8
Largazole	2.5	4.2	2.8	228
1	2.0	3.4	2.6	255
2	42	70	42	∼10000
3	13	21	15	1500

[a]Reported in ref 26.

DOI: 10.1021/acs.biochem.5b00010
Biochemistry 2015, 54, 2126−2135

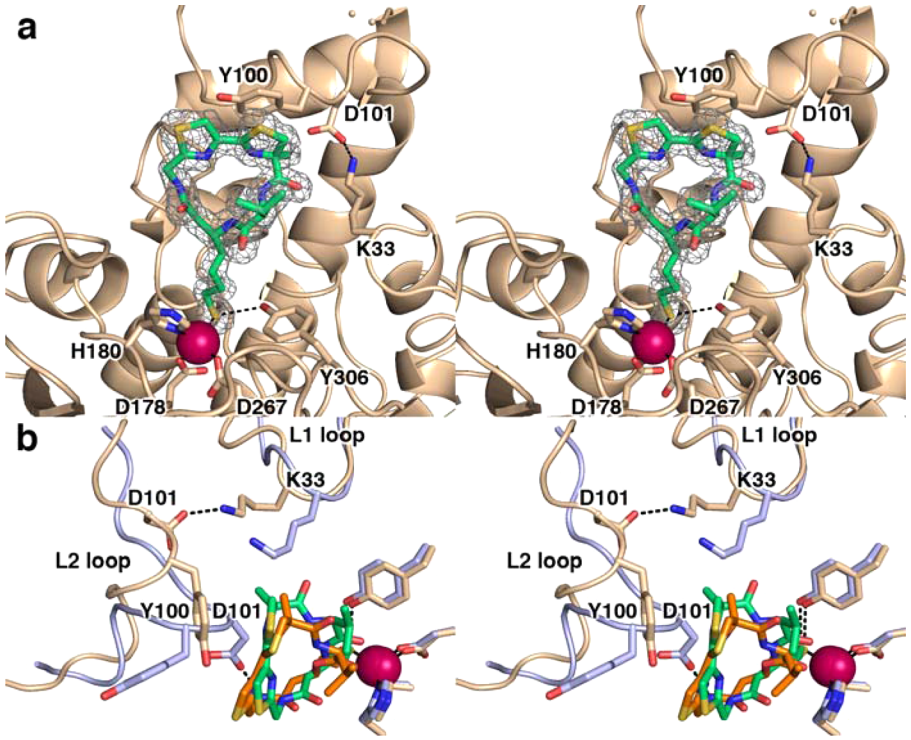

Figure 2. (a) Simulated annealing omit map of **1** bound in the active site of HDAC8 (monomer A, contoured at 3.0σ). Atomic color codes are as follows: wheat (protein) or green (inhibitor) for C, blue for N, red for O, gold for S, and Zn^{2+} as a magenta sphere. Metal coordination and selected hydrogen bond interactions are shown as solid black and dashed black lines, respectively. Wheat-colored dots indicate the disordered D87–D92 segment in the L2 loop. (b) Superposition of the HDAC8–Largazole and HDAC8–**1** complexes (monomer A of each). Significant conformational changes of the L2 loop (especially for Y100 and D101) accommodate a slightly different orientation of the macrocycle in the active site, such that the macrocycle pivots by ~25° around an axis roughly defined by the Zn^{2+}-bound thiolate and the thiazole–thiazoline bond. The HDAC8–**1** complex is color coded as in panel a; for the HDAC8–Largazole complex, light blue (protein) or orange (Largazole) for C.

interactions are similarly observed in the HDAC8–Largazole complex.

HDAC8–2 Complex. The overall structure of the HDAC8–**2** complex determined at 2.18 Å resolution is very similar to that of the HDAC8–**1** complex (rmsds of 0.16 Å for 359 Cα atoms and 0.24 Å for 356 Cα atoms in monomers A and B, respectively). The geometry of thiolate–Zn^{2+} coordination is comparable to that observed for the binding of **1**, with an average S–Zn^{2+} distance of 2.4 Å, a C–S–Zn^{2+} angle of 95°, and a C–C–S–Zn^{2+} dihedral angle of 113°; Y306 donates a hydrogen bond to the thiolate group (Figure 4a). The Zn^{2+} ion is coordinated in distorted tetrahedral fashion with ligand–Zn^{2+}–ligand angles in the range of 101–119°. The ester-to-amide substitution similarly rigidifies the macrocycle with a nearly planar linkage (amide dihedral angle of 179°). Solvent-mediated hydrogen bond contacts with active site residues are similar to those observed in the HDAC–**1** complex.

Significantly, the thiazole-to-pyridine substitution in **2** does not perturb the overall conformation of the macrocyclic peptide, and the pyridine ring adopts a similar orientation with respect to the thiazoline ring (S–C–C–C dihedral angles of 26°, 22°, and 25° for Largazole, **1**, and **2**, respectively). The pyridine ring of **2** does not interact with any surrounding residues or water molecules.

Conformational differences observed for loops L1 and L2 in the HDAC8–**1** complex are similarly observed in the HDAC8–**2** complex (Figure 4b), including the hydrogen bonds between K33 and D101, D101 and Y154 in monomer A and K33 of monomer B and the carbonyl group close to the thiazoline ring of **2** in both monomers A and B. Additionally, loop L2 in monomer B is more disordered than in monomer A, but modeled segments adopt a conformation similar to that observed in the HDAC8–**1** complex.

HDAC8–3 Complex. The overall structure of the HDAC8–**3** complex determined at 2.39 Å resolution is similar to that of the complex with **2**; as these complexes are compared, monomer A in one is overall more similar to monomer B in the other (rmsds of 0.19 Å for 347 Cα atoms in monomers A and B and 0.22 Å for 357 Cα atoms in monomers B and A of the complexes with **3** and **2**, respectively). The geometry of thiolate–Zn^{2+} coordination is slightly different, with an average S–Zn^{2+} distance of 2.4 Å, a C–S–Zn^{2+} angle of 92°, and a C–C–S–Zn^{2+} dihedral angle of 108°; ligand–Zn^{2+}–ligand angles are in the range of 91–129°, and the metal coordination polyhedron exhibits distorted tetrahedral geometry. An electron density map of the inhibitor is shown in Figure 5a. As observed for **1** and **2**, the ester-to-amide substitution rigidifies a planar conformation (amide dihedral angle of 180°), and the alternative substitution pattern on the newly introduced pyridine ring does not perturb the overall conformation of the peptide macrocycle (the thiazoline–pyridine S–C–C–C dihedral angle is 19°). A superposition of the HDAC8 complexes with **2** and **3** is found in Figure 5b.

As observed in the HDAC8–**2** complex, loop L2 (including Y100 and D101) is positioned similarly to interact with **3** in the HDAC8–**3** complex. However, in the complex with **3**, the side chain of K33 is disordered in both monomers A and B and therefore does not interact with D101. As observed in the structures of complexes with **1** and **2**, the L2 loop exhibits greater disorder in one monomer (monomer A in this

DOI: 10.1021/acs.biochem.5b00010
Biochemistry 2015, 54, 2126–2135

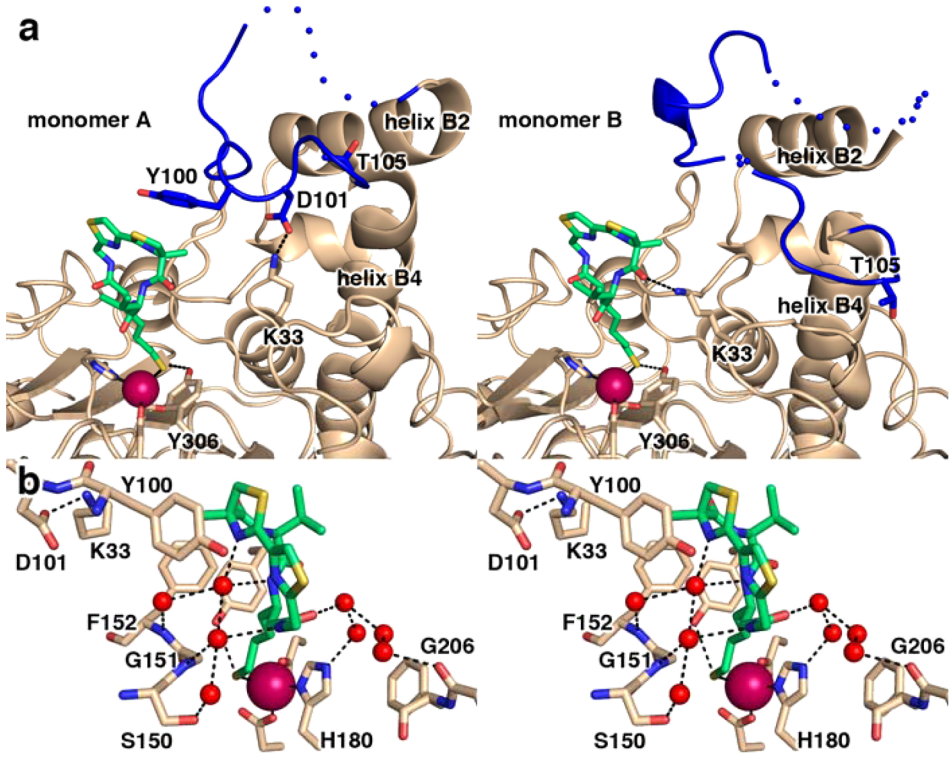

Figure 3. (a) Side-by-side comparison of monomers A and B of the HDAC8−**1** complex reveals significant conformational differences for the L2 loop involving the partial unwinding of helix B4, as noted by the position of T105. Atoms are color coded as in Figure 2a, except the L2 loop is colored blue. Dotted lines indicate the disordered D87−D92 segment and the disordered E85−D89 and G99−Y100 segments in the L2 loops of monomers A and B, respectively. (b) Close-up stereoview of the HDAC8−**1** complex showing active site water molecules (red spheres) that make bridging hydrogen bond interactions between **1** and the protein.

structure) than in the other. Monomer B of the HDAC8−**3** complex similarly differs from monomer A in terms of conformational differences in loops L1 and L2 as well as helix B2, as described above for the complexes with **1** and **2**.

DISCUSSION

The structures reported herein show that chemical modifications maintaining the 16-membered ring of the macrocyclic skeleton of Largazole are readily accommodated in the active site of HDAC8. The common feature of **1**−**3** is the ester-to-amide substitution that converts the macrocyclic depsipeptide into a peptide. This has relatively little effect on the overall conformation of the macrocyclic skeleton, even though the ester group of Largazole is distorted 9° from planarity whereas the amide group of each Largazole analogue is nearly perfectly planar with a *trans* configuration. Although the peptide macrocycle of each analogue pivots by ∼25° in the HDAC8 active site relative to Largazole (Figure 2b), this structural change has relatively little consequence for inhibitory potency against HDAC8 because the IC_{50} values for Largazole and **1** are 228 and 255 nM, respectively.[26] Additionally, this structural change is readily tolerated with regard to HDAC1−HDAC3, each of which is inhibited with comparable low-nanomolar potency by Largazole and **1** (Table 2).[26]

While the amide substitution in the 16-membered macrocyclic ring of Largazole preserves inhibitory potency, further derivatization of the macrocycle skeleton by the substitution of a pyridine ring in **2** and **3** compared with the thiazole ring of **1** moderately and slightly compromises inhibitory activity, respectively, even though this substitution does not appear to perturb the overall conformation of the macrocycle (Figures 4b and 5b). Compound **2** exhibits an ∼20−40-fold loss of inhibitory potency against HDAC1−HDAC3 and HDAC8, whereas **3** exhibits an ∼6-fold loss of inhibitory potency against these isozymes (Table 2).[26] In contrast, a pyridine ring substitution in the parent depsipeptide macrocycle enhances inhibitory potency.[19] Perhaps some degree of macrocycle flexibility is required to accommodate the substituted pyridine ring (the macrocycle ester linkage is slightly more flexible than an amide linkage). This could explain why **3** is slightly less potent than **1**. However, there is no obvious explanation for the loss of inhibitory potency of **2** relative to that of **3** (Table 2), because both appear to be readily accommodated in the HDAC8 active site based on the crystal structures shown in Figures 4 and 5.

If macrocycle flexibility is desirable, then the substitution of a more flexible ketone linkage for the depsipeptide ester linkage might allow further derivatization of the macrocycle skeleton with retention or enhancement of inhibitory potency. Additionally, given that substitution of the thiazoline ring with a tetrazole ring yields an analogue with inhibitory activity comparable to that of Largazole,[37] it is possible that further derivatization of the thiazoline−thiazole moiety will similarly preserve inhibitory activity as long as the overall macrocycle conformation is retained. Because the thiazoline−thiazole ring system of **1** and the thiazoline−pyridine ring systems of **2** and **3** are solvent-exposed, such derivatization could include the attachment of pendant functional groups for the capture of additional affinity interactions in the outer active site cleft.

The most important feature of HDAC inhibition by depsipeptide and peptide macrocycles is the strong coordination interaction between the inhibitor thiol group and the active

DOI: 10.1021/acs.biochem.5b00010
Biochemistry 2015, 54, 2126−2135

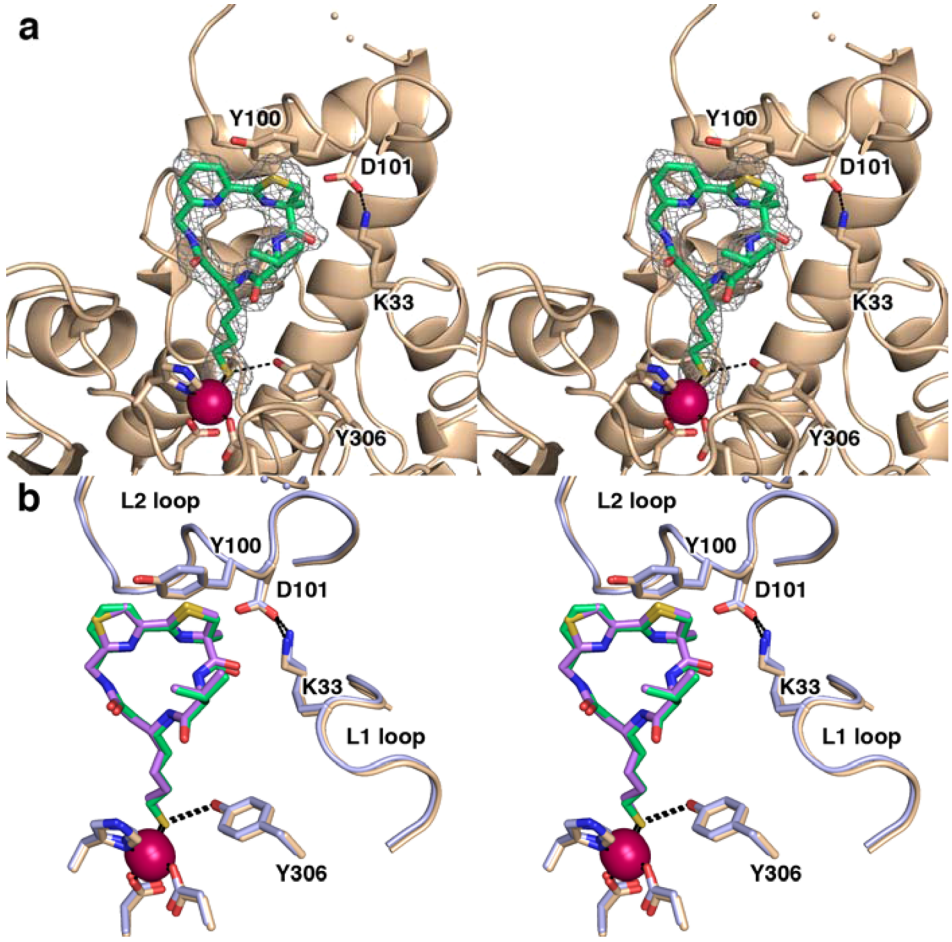

Figure 4. (a) Simulated annealing omit map of **2** bound in the active site of HDAC8 (monomer A, contoured at 2.8σ). Atomic color codes are as follows: wheat (protein) or green (inhibitor) for C, blue for N, red for O, gold for S, and Zn^{2+} as a magenta sphere. Metal coordination and selected hydrogen bond interactions are shown as solid black and dashed black lines, respectively. Wheat-colored dotted lines indicate the disordered D88–P91 segment in loop L2. (b) Superposition of HDAC8 complexes (monomer A) reveals that Largazole analogues **2** and **1** adopt similar binding modes, and the flexible L1 and L2 loops adopt similar conformations. The HDAC8–**2** complex is color coded as in panel a; for the HDAC8–**1** complex, light blue (protein) or violet (analogue **1**) for C.

site Zn^{2+} ion. In the structures of HDAC8 complexes with **1**–**3**, the S–Zn^{2+} coordination distance is 2.3–2.4 Å, which is the ideal coordination bond length[36] and is comparable to that observed in the HDAC8–Largazole complex.[18] The coordination geometry of the active site Zn^{2+} ion is tetrahedral or distorted tetrahedral, with average deviations from ideal tetrahedral geometry of 6°, 6°, and 13° for **1**–**3**, respectively. For the HDAC8–Largazole complex, the average deviation from ideal tetrahedral Zn^{2+} coordination geometry is 4°. The deviation from ideal coordination geometry is greatest in the HDAC8–**3** complex, but this could be a consequence of the lower resolution of this crystal structure compared with the resolution of the others.

Some differences are observed in the conformations of the thiol side chain of Largazole and its derivatives, and these differences may influence inhibitory potency. The thiol side chain extends from the macrocycle skeleton into the active site tunnel to allow S–Zn^{2+} coordination, and the chemical structure of this side chain, which includes a *trans* double bond between the Cβ and Cγ atoms, is identical in all derivatives (Figure 1). In the HDAC8 complexes with Largazole and **1**, the overall side chain conformation is bent such that the Cβ–Cγ–Cδ–Cε torsion angles are anticlinal, with average values of −122° and −124°, respectively. In contrast, the thiol side chains of **2** and **3** tend toward antiperiplanar conformations in their complexes with HDAC8, with average Cβ–Cγ–Cδ–Cε torsion angles of −166° and −168°, respectively. Thus, it appears that more potent inhibitory affinity is achieved for macrocyclic thiols that can bind in the enzyme active site and retain the anticlinal thiol side chain conformation, as initially observed in the HDAC8–Largazole complex.[18] If the anticlinal-to-antiperiplanar conformational change of the thiol side chain is caused by the pyridine substitutions in the macrocyclic rings of **2** and **3**, it is not clear from the structures of their HDAC8 complexes how this occurs.

Strikingly, the binding of Largazole analogues in the active site of HDAC8 reveals new features regarding the conformational flexibility of loops flanking the active site and the role of these loops in accommodating the binding of large, structurally similar ligands. Such conformational flexibility presumably accompanies the binding of protein substrates *in vivo* and as such may play an important role in governing substrate specificity. Surprisingly, the binding of all three Largazole analogues triggers significant conformational changes in the L2 loop that propagate through to loop L1 and helix B2; moreover, these conformational changes differ from those observed in the HDAC8–Largazole complex.[18] It is particularly noteworthy to

DOI: 10.1021/acs.biochem.5b00010
Biochemistry 2015, 54, 2126–2135

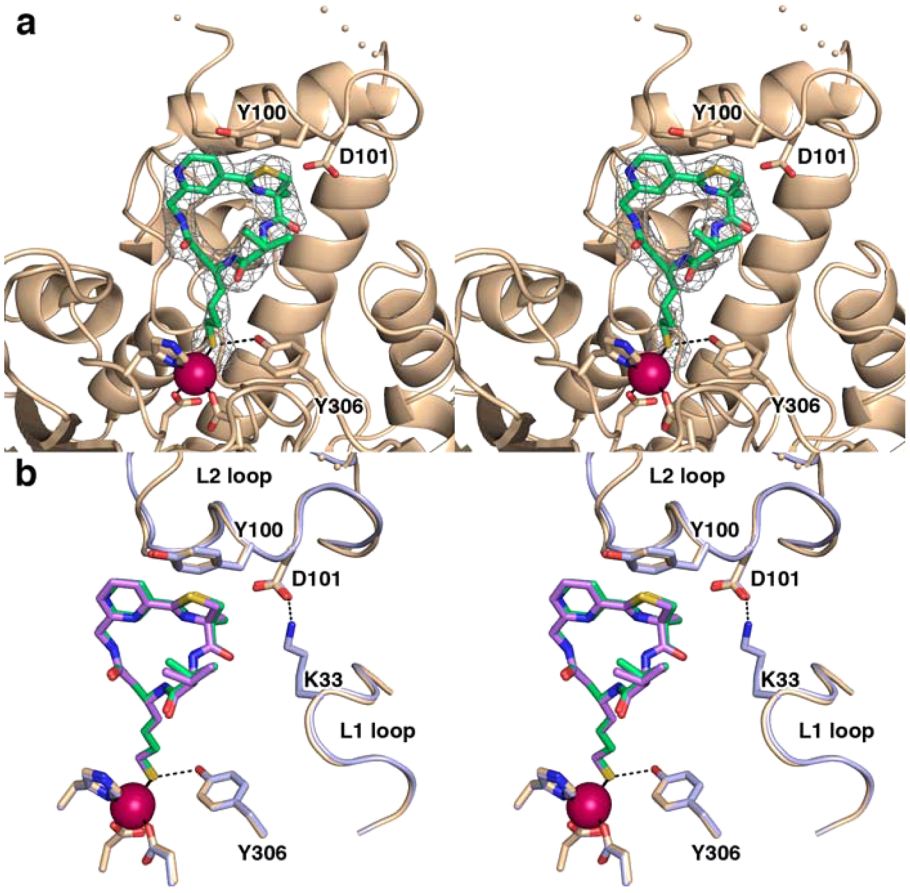

Figure 5. (a) Simulated annealing omit map of **3** bound in the active site of HDAC8 (monomer B, contoured at 2.8σ). Atomic color codes are as follows: wheat (protein) or green (inhibitor) for C, blue for N, red for O, gold for S, and Zn^{2+} as a magenta sphere. Metal coordination and selected hydrogen bond interactions are shown as solid black and dashed black lines, respectively. Wheat-colored dotted lines indicate the disordered D87–D92 segment in loop L2. (b) Largazole analogues **3** and **2** bind similarly in the active site of HDAC8. While the L2 loops adopt slightly different conformations, Y100 and D101 are positioned similarly in each complex. The HDAC8–**3** complex is color coded as in panel a; for the HDAC8–**2** complex (monomer A), light blue (protein) or violet (analogue **2**) for C.

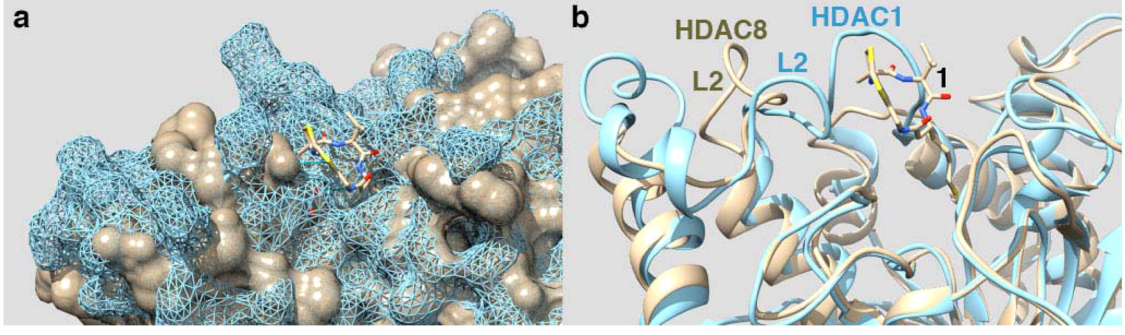

Figure 6. (a) Surface representation of the HDAC8–**1** complex (brown) and HDAC1 (blue mesh). (b) Cartoon representation of the superposition in panel a, with the position of flexible loop L2 in HDAC1 and HDAC8 indicated.

see such differences in protein conformational changes that accommodate the binding of isosteric ligands, and it is even more noteworthy to see such differences in the binding of the same ligand to independent monomers in the same crystal.

Loop L2 of HDAC8 is already known to undergo conformational changes to accommodate the binding of different ligands, and residues contained in this loop are usually characterized by higher thermal *B* factors and/or a lack of clear electron density. However, in this array of structures, the rearrangement of this loop is more pronounced than that usually observed. For example, the side chain of D101, which usually hydrogen bonds with bound substrates or inhibitors, is shifted by ~7 Å from the macrocycle, such that adjacent residue Y100 now associates more closely with the macrocycle (Figures 2a, 4a, and 5a). Interestingly, recent molecular dynamics simulations suggest that loops L1 and L2 can interact through K33 and D87/D88/D89.[38] Here, we show that a direct interaction between loops L1 and L2 can also be made between K33 and D101, as observed in monomers A of the complexes with **1** and **2**. Presumably, such L1–L2 loop interactions play an important role in governing specificity and affinity in the binding of substrates and inhibitors.

DOI: 10.1021/acs.biochem.5b00010
Biochemistry 2015, 54, 2126–2135

These results are consistent with the high conformational flexibility of loops L1 and L2 of HDAC8 observed in crystallographic[18,27,39,40] and molecular dynamics (MD) studies.[38,41] In comparison, the loops surrounding the active site of HDAC1, which is a more promising drug target and binds Largazole and its analogues ~200 times more tightly, are much less flexible in MD simulations.[42] In the absence of a crystal structure of a complex between HDAC1 and a Largazole derivative, we analyzed the structural relationship between the HDAC8−**1** complex and the structure of HDAC1 complexed with the ELM2 and SANT domains of metastasis-associated protein 1 (MTA1).[43] Figure 6a shows the surface representation of the overlay of HDAC1 in blue mesh and chain A of the HDAC8−**1** complex in light brown in the area around the binding site; the cartoon representation in Figure 6b is similarly color-coded. It can be seen that loops L1 and L2 adopt different conformations that enhance the shape complementarity to **1**, even though the overall degree of structural similarity is very high. Loop L1 in HDAC1, which is four residues longer and more rigid than the corresponding L1 loop in HDAC8, protrudes on one side of the active site mouth as indicated by the blue mesh in Figure 6a. Additional interactions with the isopropyl group and the amide functionality of Largazole analogues, which are maintained during extensive MD simulations,[26] rationalize the increased binding affinity of the Largazole analogues for HDAC1. It is possible, too, that the decreased flexibility of loops L1 and L2 of HDAC1 may decrease the conformational entropic cost of inhibitor binding. These results reinforce the importance of HDAC surface interactions for the binding and isozyme selectivity of Largazole and related depsipeptide inhibitors.

CONCLUDING REMARKS

As observed in previous structural studies,[27,29,39,40] active site loops, especially loop L2, play an important role in the binding of small hydroxamate inhibitors to HDAC8. These loops play an even more important role in accommodating the 16-membered ring of the macrocyclic depsipeptide inhibitor Largazole and its amide derivatives **1**−**3**. While residues in the L2 loop such as D101 are capable of hydrogen bonding with the Largazole macrocycle, the binding of the three amide derivatives shows that a hydrogen bond interaction with D101 need not be conserved to maintain inhibitory potency. Indeed, this study shows that loop L2 exhibits remarkable flexibility to better accommodate structural variations in the macrocycle skeleton, all while maintaining ideal S−Zn^{2+} coordination geometry by the thiol side chain. Strikingly, alternative loop conformations accommodate the binding of isosteric ligands, or even the same ligand, to independent monomers in the same crystal. Such flexibility in both loops L1 and L2 accommodates diverse protein substrates in the HDAC8 active site. Crystal structures of HDAC8 complexes with Largazole and its macrocyclic analogues provide an unprecedented view of how such molecular accommodation is achieved.

ASSOCIATED CONTENT

Accession Codes

The atomic coordinates and the crystallographic structure factors of HDAC8 complexes with **1**−**3** have been deposited in the Protein Data Bank (www.rcsb.org) as entries 4RN0, 4RN1, and 4RN2, respectively.

AUTHOR INFORMATION

Corresponding Author

*E-mail: chris@sas.upenn.edu. Telephone: (215) 898-5714.

Funding

We thank the National Institutes of Health for Grants GM49758 (to D.W.C.) and CA152314 (to R.M.W. and O.W.) in support of this research.

Notes

The authors declare no competing financial interest.

ACKNOWLEDGMENTS

We thank the National Synchrotron Light Source at Brookhaven National Laboratory for access to beamline X29 for X-ray crystallographic data collection. Additionally, we thank Dr. A. Lebedev for helpful discussions.

REFERENCES

(1) De Ruijter, A. J. M., van Gennip, A. H., Caron, H. N., Kemp, S., and van Kuilenburg, A. B. P. (2003) Histone deacetylases (HDACs): Characterization of the classical HDAC family. *Biochem. J. 370*, 737−749.

(2) Gregoretti, I. V., Lee, Y.-M., and Goodson, H. V. (2004) Molecular evolution of the histone deacetylase family: Functional implications of phylogenetic analysis. *J. Mol. Biol. 338*, 17−31.

(3) Gantt, S. L., Gattis, S. G., and Fierke, C. A. (2006) Catalytic activity and inhibition of human histone deacetylase 8 is dependent on the identity of the active site metal ion. *Biochemistry 45*, 6170−6178.

(4) Genshaft, A., Moser, J.-A. S., D'Antonio, E. L., Bowman, C. M., and Christianson, D. W. (2013) Energetically unfavorable amide conformations for N6-acetyllysine side chains in refined protein structures. *Proteins: Struct., Funct., Bioinf. 81*, 1051−1057.

(5) Lombardi, P. M., Cole, K. E., Dowling, D. P., and Christianson, D. W. (2011) Structure, mechanism, and inhibition of histone deacetylases and related metalloenzymes. *Curr. Opin. Struct. Biol. 21*, 735−743.

(6) Wolfson, N. A., Pitcairn, C. A., and Fierke, C. A. (2013) HDAC8 substrates: Histones and beyond. *Biopolymers 99*, 112−126.

(7) Haberland, M., Montgomery, R. L., and Olson, E. N. (2009) The many roles of histone deacetylases in development and physiology: Implications for disease and therapy. *Nat. Rev. Genet. 10*, 32−42.

(8) Emanuele, S., Lauricella, M., and Tesoriere, G. (2008) Histone deacetylase inhibitors: Apoptotic effects and clinical implications. *Int. J. Oncol. 33*, 637−646.

(9) Marks, P. A. (2010) Histone deacetylase inhibitors: A chemical genetics approach to understanding cellular functions. *Biochim. Biophys. Acta 1799*, 717−725.

(10) New, M., Olzscha, H., and La Thangue, N. B. (2012) HDAC inhibitor-based therapies: Can we interpret the code? *Mol. Oncol. 6*, 637−656.

(11) Delcuve, G. P., Khan, D. H., and Davie, J. R. (2012) Roles of histone deacetylases in epigenetic regulation: Emerging paradigms from studies with inhibitors. *Clin. Epigenet. 4*, 5.

(12) Marks, P. A., and Breslow, R. (2007) Dimethyl sulfoxide to vorinostat: Development of this histone deacetylase inhibitor as an anticancer drug. *Nat. Biotechnol. 25*, 84−90.

(13) Mann, B. S., Johnson, J. R., Cohen, M. H., Justice, R., and Pazdur, R. (2007) FDA approval summary: Vorinostat for treatment of advanced primary cutaneous T-cell lymphoma. *Oncologist 12*, 1247−1252.

(14) Guan, P., and Fang, H. (2010) Clinical development of histone deacetylase inhibitor romidepsin. *Drug Discovery Ther. 4*, 388−391.

(15) Furumai, R., Matsuyama, A., Kobashi, N., Lee, K.-H., Nishiyama, M., Nakajima, H., Tanaka, A., Komatsu, Y., Nishino, N., Yoshida, M., and Horinouchi, S. (2002) FK228 (depsipeptide) as a natural prodrug that inhibits class I histone deacetylases. *Cancer Res. 62*, 4916−4921.

DOI: 10.1021/acs.biochem.5b00010
Biochemistry 2015, 54, 2126−2135

(16) Taori, K., Paul, V. J., and Luesch, H. (2008) Structure and activity of largazole, a potent antiproliferative agent from the Floridian marine cyanobacterium *Symploca* sp. *J. Am. Chem. Soc. 130*, 1806−1807.
(17) Ying, Y., Taori, K., Kim, H., Hong, J., and Luesch, H. (2008) Total synthesis and molecular target of largazole, a histone deacetylase inhibitor. *J. Am. Chem. Soc. 130*, 8455−8459.
(18) Cole, K. E., Dowling, D. P., Boone, M. A., Phillips, A. J., and Christianson, D. W. (2011) Structural basis of the antiproliferative activity of largazole, a depsipeptide inhibitor of the histone deacetylases. *J. Am. Chem. Soc. 133*, 12474−12477.
(19) Bowers, A. A., West, N., Newkirk, T. L., Troutman-Youngman, A. E., Schreiber, S. L., Wiest, O., Bradner, J. E., and Williams, R. M. (2009) Synthesis and histone deacetylase inhibitory activity of largazole analogs: Alteration of the zinc-binding domain and macrocyclic scaffold. *Org. Lett. 11*, 1301−1304.
(20) Bowers, A., West, N., Taunton, J., Schreiber, S. L., Bradner, J. E., and Williams, R. M. (2008) Total synthesis and biological mode of action of largazole: A potent class I histone deacetylase inhibitor. *J. Am. Chem. Soc. 130*, 11219−11222.
(21) Nasveschuk, C. G., Ungermannova, D., Liu, X., and Phillips, A. J. (2008) A concise total synthesis of largazole, solution structure, and some preliminary structure-activity relationships. *Org. Lett. 10*, 3595−3598.
(22) Ghosh, A. K., and Kulkarni, S. (2008) Enantioselective total synthesis of (+)-largazole, a potent inhibitor of histone deacetylase. *Org. Lett. 10*, 3907−3909.
(23) Guerra-Bubb, J. M., Bowers, A. A., Smith, W. B., Paranal, R., Estiu, G., Wiest, O., Bradner, J. E., and Williams, R. M. (2013) Synthesis and HDAC inhibitory activity of isosteric thiazoline-oxazole largazole analogs. *Bioorg. Med. Chem. Lett. 23*, 6025−6028.
(24) Bowers, A. A., Greshock, T. J., West, N., Estiu, G., Schreiber, S. L., Wiest, O., Williams, R. M., and Bradner, J. E. (2009) Synthesis and conformation-activity relationships of the peptide isosteres of FK228 and largazole. *J. Am. Chem. Soc. 131*, 2900−2905.
(25) Rettig, I., Koeneke, E., Trippel, F., Mueller, W. C., Burhenne, J., Kopp-Schneider, A., Fabian, J., Schober, A., Fernekorn, U., von Deimling, A., Deubzer, H. E., Milde, T., Witt, O., and Oehme, I. (2015) Selective inhibition of HDAC8 decreases neuroblastoma growth *in vitro* and *in vivo* and enhances retinoic acid-mediated differentiation. *Cell Death Dis. 6*, e1657.
(26) Clausen, D. J., Smith, W. B., Haines, B. E., Wiest, O., Bradner, J. E., and Williams, R. M. (2015) Modular synthesis and biological activity of pyridyl-based analogs of the potent class I histone deacetylase inhibitor Largazole. *Bioorg. Med. Chem.*, in press.
(27) Dowling, D. P., Gantt, S. L., Gattis, S. G., Fierke, C. A., and Christianson, D. W. (2008) Structural studies of human histone deacetylase 8 and its site-specific variants complexed with substrate and inhibitors. *Biochemistry 47*, 13554−13563.
(28) Decroos, C., Bowman, C. M., Moser, J.-A. S., Christianson, K. E., Deardorff, M. A., and Christianson, D. W. (2014) Compromised structure and function of HDAC8 mutants identified in Cornelia de Lange Syndrome spectrum disorders. *ACS Chem. Biol. 9*, 2157−2164.
(29) Vannini, A., Volpari, C., Gallinari, P., Jones, P., Mattu, M., Carfí, A., De Francesco, R., Steinkühler, C., and Di Marco, S. (2007) Substrate binding to histone deacetylases as shown by the crystal structure of the HDAC8-substrate complex. *EMBO Rep. 8*, 879−884.
(30) Otwinowski, Z., and Minor, W. (1997) Processing of X-ray diffraction data collected in oscillation mode. *Methods Enzymol. 276*, 307−326.
(31) Barends, T. R. M., and Dijkstra, B. W. (2003) *Acetobacter turbidans* α-amino acid ester hydrolase: Merohedral twinning in $P2_1$ obscured by pseudo-translational NCS. *Acta Crystallogr. D59*, 2237−2241.
(32) Winn, M. D., Ballard, C. C., Cowtan, K. D., Dodson, E. J., Emsley, P., Evans, P. R., Keegan, R. M., Krissinel, E. B., Leslie, A. G. W., McCoy, A., McNicholas, S. J., Murshudov, G. N., Pannu, N. S., Potterton, E. A., Powell, H. R., Read, R. J., Vagin, A., and Wilson, K. S. (2011) Overview of the CCP4 suite and current developments. *Acta Crystallogr. D67*, 235−242.
(33) Adams, P. D., Afonine, P. V., Bunkóczi, G., Chen, V. B., Davis, I. W., Echols, N., Headd, J. J., Hung, L. W., Kapral, G. J., Grosse-Kunstleve, R. W., McCoy, A. J., Moriarty, N. W., Oeffner, R., Read, R. J., Richardson, D. C., Richardson, J. S., Terwilliger, T. C., and Zwart, P. H. (2010) PHENIX: A comprehensive Python-based system for macromolecular structure solution. *Acta Crystallogr. D66*, 213−221.
(34) Emsley, P., Lohkamp, B., Scott, W. G., and Cowtan, K. (2010) Features and development of Coot. *Acta Crystallogr. D66*, 486−501.
(35) Lee, H., Rezai-Zadeh, N., and Seto, E. (2004) Negative regulation of histone deacetylase 8 activity by cyclic AMP-dependent protein kinase A. *Mol. Cell. Biol. 24*, 765−773.
(36) Chakrabarti, P. (1989) Geometry of interaction of metal ions with sulfur-containing ligands in protein structures. *Biochemistry 28*, 6081−6085.
(37) Li, X., Tu, Z., Li, H., Liu, C., Li, Z., Sun, Q., Yao, Y., Liu, J., and Jiang, S. (2013) Biological evaluation of new largazole analogues: Alteration of macrocyclic scaffold with click chemistry. *ACS Med. Chem. Lett. 4*, 132−136.
(38) Kunze, M. B. A., Wright, D. W., Werbeck, N. D., Kirkpatrick, J., Coveney, P. V., and Hansen, D. F. (2013) Loop interactions and dynamics tune the enzymatic activity of the human histone deacetylase 8. *J. Am. Chem. Soc. 135*, 17862−17868.
(39) Somoza, J. R., Skene, R. J., Katz, B. A., Mol, C., Ho, J. D., Jennings, A. J., Luong, C., Arvai, A., Buggy, J. J., Chi, E., Tang, J., Sang, B.-C., Verner, E., Wynands, R., Leahy, E. M., Dougan, D. R., Snell, G., Navre, M., Knuth, M. W., Swanson, R. V., McRee, D. E., and Tari, L. W. (2004) Structural snapshots of human HDAC8 provide insights into the class I histone deacetylases. *Structure 12*, 1325−1334.
(40) Vannini, A., Volpari, C., Filocamo, G., Casavola, E. C., Brunetti, M., Renzoni, D., Chakravarty, P., Paolini, C., De Francesco, R., Gallinari, P., Steinkühler, C., and Di Marco, S. (2004) Crystal structure of a eukaryotic zinc-dependent histone deacetylase, human HDAC8, complexed with a hydroxamic acid inhibitor. *Proc. Natl. Acad. Sci. U.S.A. 101*, 15064−15069.
(41) Estiu, G., West, N., Mazitschek, R., Greenberg, E., Bradner, J. E., and Wiest, O. (2010) On the inhibition of histone deacetylase 8. *Bioorg. Med. Chem. 18*, 4103−4110.
(42) Weerasinghe, S. V. W., Estiu, G., Wiest, O., and Pflum, M. K. H. (2008) Residues in the 11 Å channel of histone deacetylase 1 promote catalytic activity: Implications for designing isoform-selective histone deacetylase inhibitors. *J. Med. Chem. 51*, 5542−5551.
(43) Millard, C. J., Watson, P. J., Celardo, I., Gordiyenko, Y., Cowley, S. M., Robinson, C. V., Fairall, L., and Schwabe, J. W. R. (2013) Class I HDACs share a common mechanism of regulation by inositol phosphates. *Mol. Cell 51*, 57−67.

DOI: 10.1021/acs.biochem.5b00010
Biochemistry 2015, 54, 2126−2135